

**CALIBRATION OF THE NEAR-SURFACE SEISMIC STRUCTURE IN THE SCEC
COMMUNITY VELOCITY MODEL VERSION S**

Kim Olsen and Te-Yang Yeh

Department of Earth and Environmental Sciences
San Diego State University

Abstract

We have estimated the thickness distribution of a geotechnical layer in the SCEC CVM-S4.26M01 (updated with recent ambient noise results) that generates the least-biased fit between 3D 0-1 Hz physics-based ground motion simulations and strong motion data in the greater Los Angeles area, CA, for 7 M_w 4.4-5.4 earthquakes. Outside the basins, the optimal GTL thickness distribution shows strong spatial variation, generally increasing from near 0 m at the edges of the basins to values of 1,000 m or larger at distances of about 10-50 km, in particular toward the northeast, east and southeast.

Introduction

The near-surface seismic structure to a depth of about 1,000 m, particularly the shear-wave velocity (V_s), can strongly affect the propagation of seismic waves, and therefore must be accurately calibrated for ground motion simulations used in seismic hazard assessment. The V_s structure of the material deeper than about 1,000 m are typically reasonably-well determined by tomography studies. However, at shallower depths, when constraints are missing from borehole studies, geotechnical measurements, and water and oil wells, typically at rock sites outside the sedimentary basins, the material parameters are often poorly characterized.

When the alluded geological constraints are not available, models, such as the Statewide California Earthquake Center (SCEC) Community Velocity Models (CVMs), default to regional tomographic estimates that do not resolve the uppermost V_s values, and therefore deliver unrealistically high shallow V_s estimates. The SCEC Unified Community Velocity model (UCVM) software includes a method to incorporate the near-surface earth structure by applying a generic overlay based on measurements of time-averaged V_s in the top 30 m (V_{s30}) to taper the upper part of the model to merge with tomography at a depth of 350 m, which can be applied to any of the velocity models accessible through UCVM. However, Hu et al. (2022) used 3D deterministic simulations in the Los Angeles area with the SCEC CVM-S4.26.M01 model to show that low-frequency (< 1 Hz) ground motions at sites where the material properties in the top 350 m are modified by the generic overlay (“taper”) significantly underpredict those from the 2014 M_w 5.1 La Habra earthquake. On the other hand, Hu et al. (2022) showed that extending the V_{s30} -based taper of the shallow velocities to a depth of 700-1,000 meters improved the fit between their synthetics and seismic data at those sites significantly, without compromising the fit at well constrained sites.

In addition to recommending that the taper depth be extended, Hu al. (2022) also proposed further work. Specifically, they suggested that their results be checked using additional ground motion metrics, and including multiple earthquakes generating waves propagating into the basins from different azimuths, which has been shown to affect amplification patterns (Olsen, 2000). Moreover, although they found improvements using a uniform tapering depth, they observed some spatial variabilities that, if accounted for, may further improve their method. Here, we further analyze the near-surface velocities in the SCEC CVM-S4.26.M01 outside the greater Los Angeles basins, with the goal of improving the fit between synthetic and observed seismic data. Toward this goal, we simulate 0-1 Hz physics-based wave propagation for 7 well-recorded events with magnitudes between 4.4 and 5.4 and varying azimuth with respect to the Los Angeles area (see Figure 1), and estimate a spatially-variable distribution of optimal tapering depths outside the sedimentary basins. Finally, we assess the how well the long-period ground motions were predicted in the sedimentary basins for the 7 events, and provide recommendations for further work.

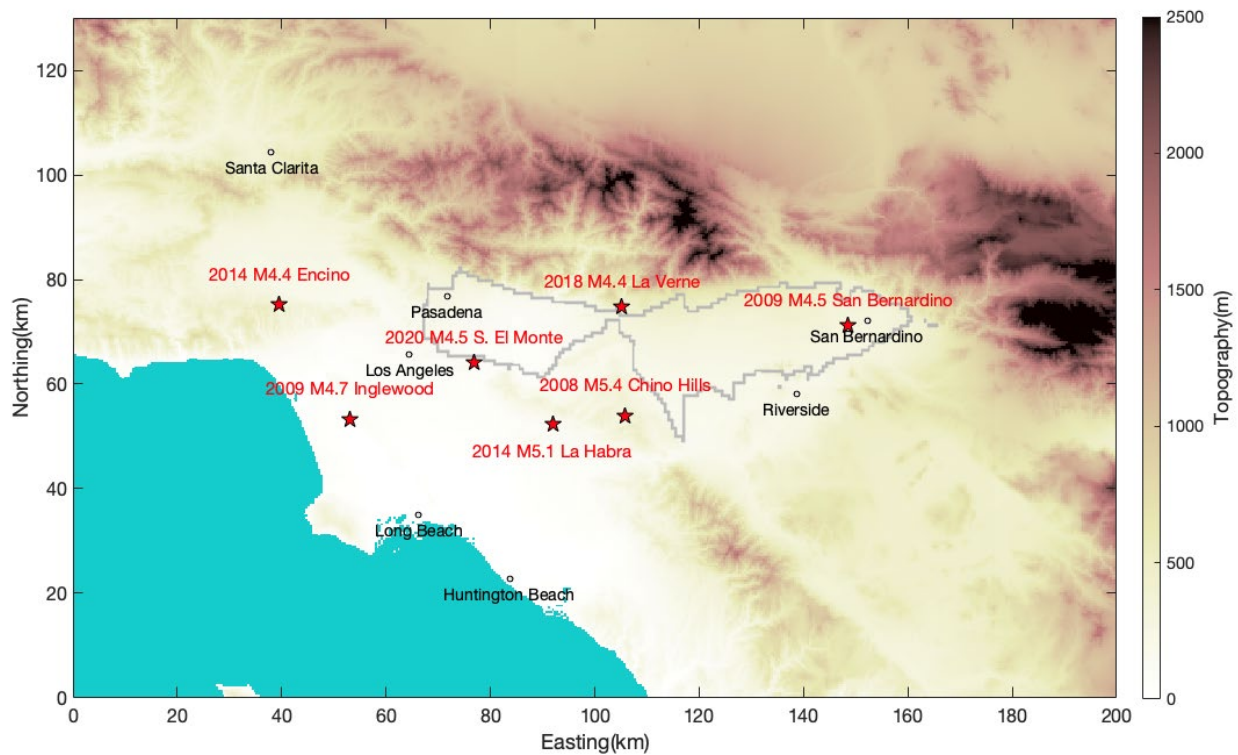


Figure 1. Map showing the simulation domain and locations of the events included in this study. The thick gray line depicts the boundary of the SGSB model imaged by Li et al. (2023).

Numerical Method

We use the 4th-order accurate finite-difference code AWP-ODC (Cui et al., 2010) for our simulations. In order to reduce the computational cost, we used 3 velocity meshes separated vertically with a factor-of-three increase in grid spacing with depth via a discontinuous mesh approach (Nie et al., 2017). Topography is modeled used the curvilinear grid approach by O’Reilly et al. (2022).

Table 1 provides details of the numerical simulations. We used a minimum shear wave velocity of 180 m/s in the top block, ensuring at least 6.7 points per minimum wavelength (O’Reilly et al., 2022).

Velocity and Anelastic Attenuation Model

Our target reference model in this study is the SCEC CVM version 4.26-M01 (CVM-S in the following, Small et al., 2017). We extract a domain of dimensions 200 km (X) x 130 km (Y) x 100 km (Z), covering the entire Los Angeles basin (LAB), San Fernando basin (SFB), San Gabriel basin (SGB), Chino basin (CB), and San Bernardino basin (SBB), as well as the surrounding areas (Figure 1). Following Olsen et al. (2003), we assume $Q_{s,0}$ to be proportional to the local S-wave speed, $Q_{s,0} = kV_s$, where k is a parameter specific to the study area. We adopt the same model as Hu et al. (2022) for the anelastic attenuation, namely $Q_s=0.1V_s$ (V_s in m/s) and $Q_p=2Q_s$.

Goodness-of-fit (GOF) Measure

We use the Fourier amplitude spectral (FAS) bias as a quantification of model performance, defined as

$$FAS_{bias}(f) = \log_{10} \frac{FAS_{model}(f)}{FAS_{data}(f)},$$

where $FAS_{model}(f)$ and $FAS_{data}(f)$ are the root-mean-squared horizontal spectra of the simulated and observed waveforms, respectively. Before computing the FAS bias, all spectra were smoothed using the Konno-Ohmachi method with a bandwidth of 40 (Konno and Ohmachi, 1998). Finally, we compute the mean of the FAS bias values over the frequency points between 0.3 - 1 Hz.

Table 1. Simulation parameters.

Model dimensions	Top mesh: 6,696 x 4,320 x 416 Middle mesh: 2,232 x 1,440 x 480 Bottom mesh: 744 x 480 x 160
Grid spacings	30 m: Free surface to 12.42 km depth 90 m: 12.21 km depth to 55.32 km depth 270 m: 54.69 km depth to 96.62 km depth
Minimum V_s	180 m/s
Maximum frequency	1 Hz
Timestep	0.0015 s
Simulated time length	100 s

Near-surface Geotechnical Layer (GTL)

We follow the approach of Hu et al. (2022) to calibrate the near-surface velocity structure within our model domain. This calibration entails replacing the velocity model extracted from the SCEC CVM-S, from the free surface to a given tapering depth (z_T) with V_s , V_p and density computed using the formulations of Ely et al. (2010) along with local V_{S30} information. This approach provides a smooth transition between the near-surface velocity structures and the original model. We used measured V_{S30} values wherever available, and the values from Thompson et al. (2018) elsewhere.

To implement the GTL, we use the taper function proposed by Ely et al. (2010), which considers the local V_{s30} value, given by

$$\begin{aligned}
 z &= z'/z_T \\
 f(z) &= z + b(z - z^2) \\
 g(z) &= a - az + c(z^2 + 2\sqrt{z} - 3z) \\
 V_S(z) &= f(z)V_{ST} + g(z)V_{S30} \\
 V_P(x) &= f(z)V_{PT} + g(z)P(V_{S30}) \\
 \rho(z) &= R(V_P)
 \end{aligned} \tag{1}$$

where z is a normalized depth, z' is depth, z_T is a transition depth, and V_p and V_s are computed using linear combinations of $f(z)$ and $g(z)$ functions along with V_{PT} and V_{ST} , which are V_P and V_S , respectively, in the original model at z_T . P and R are functions used for the V_P scaling law from the Brocher (2005) and Nafe-Drake law, respectively. Here, we use the coefficients $a=1/2$, $b=2/3$, and $c=3/2$ in Eq. (1), consistent with Ely et al. (2010).

Due to the simplification in the formulation of Ely et al. (2010), the resulting V_{s30} of the V_s taper does not always match the input V_{s30} value. We corrected for this discrepancy in all models with the GTL implemented by replacing the V_s profile in the top 30 m with the re-scaled V_s profile for generic rock sites from Boore and Joyner (1997), defined as

$$V_{sc}(z) = (V_{sBJ1997}(z)/617)V_{S30}, z < 30m \tag{2}$$

where V_{sc} is the corrected V_s profile, $V_{sBJ1997}$ is the V_s profile for generic rock sites from Boore and Joyner (1997), and V_{s30} is the targeted V_{s30} value to be matched. The scale factor (617 m/s) used here is the V_{s30} of $V_{sBJ1997}$, which is given by

$$\begin{aligned}
 V_{sBJ1997}(z) &= 245m/s, z \leq 1m \\
 V_{sBJ1997}(z) &= 2206(z/1000)^{0.272}m/s, 1 < z \leq 30m,
 \end{aligned} \tag{3}$$

where the depth is in meters. To avoid creating a velocity contrast at 30 m depth, we linearly transition V_{sc} at 30 m [$V_{sc}(30)$] to the existing V_s at a depth of 60 m [$V_{sc}(60)$] that is,

$$V_{s_c}(z) = V_{s_c}(30) + \frac{V_s(60) - V_{s_c}(30)}{(60 - 30)}(z - 30), 30m \leq z \leq 60m. (4)$$

V_p and density were computed from V_{sc} using empirical relations from Brocher (2005). Note that in the simulations with a grid spacing of 30 m, the velocities were computed by the harmonic average of velocity values within the depth range associated with each grid.

Ground Motion Simulations

We simulate 7 M_w 4.4-5.4 events (2014 M_w 4.4 Encino, 2009 M_w 4.7 Inglewood, 2020 M_w 4.5 South El Monte, 2018 M_w 4.4 La Verne, 2009 M_w 4.5 San Bernardino, M_w 5.1 2014 La Habra, and the 2008 M_w 5.4 Chino Hills earthquakes, see Fig. 1) to further calibrate the tapering depths in the greater Los Angeles area. The La Habra and Chino Hills events are simulated using the finite fault sources described in Hu et al. (2022) and Shao et al. (2012), respectively, while the remaining events (M_w 4.4-4.7) are considered sufficiently small to be simulated using point sources for frequencies up to 1 Hz. All point sources use a Brune-type moment-rate function and a stress drop of 3 MPa.

We follow the approach of Hu et al. (2022) and classify site locations based on surface V_s in the original CVM-S into type A (surface $V_s \leq 1000$ m/s) and type B (surface $V_s > 1000$ m/s) sites. Figure 2 shows the location of the source and stations of types A and B.

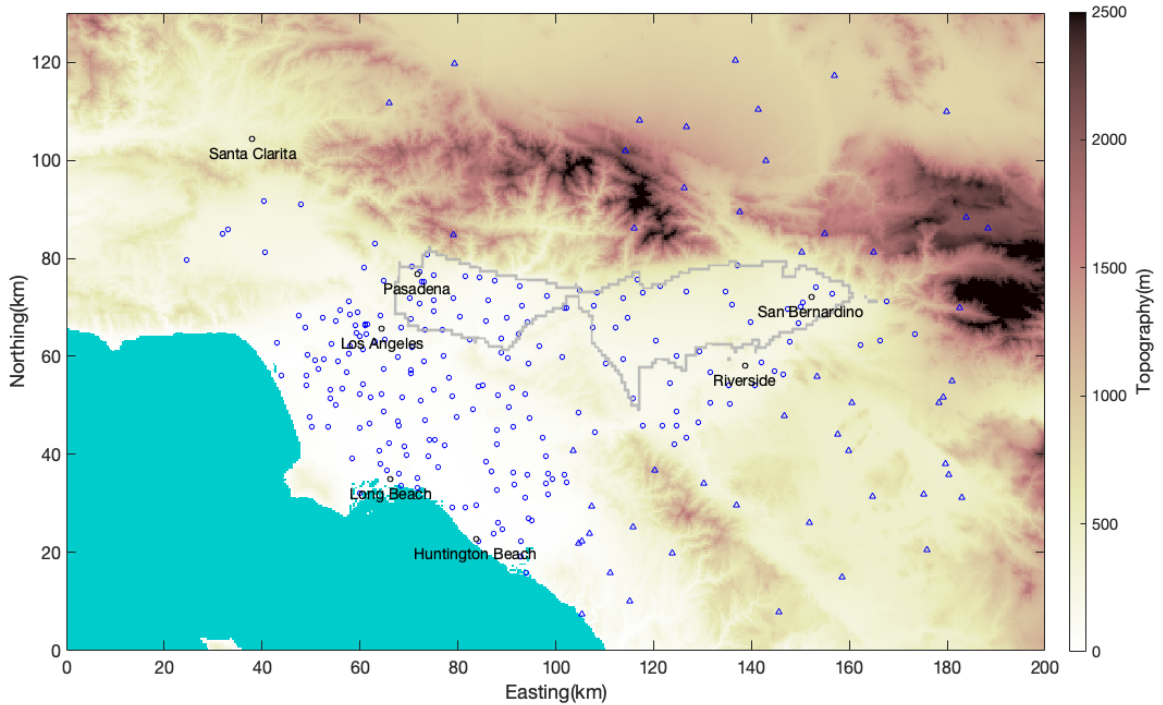


Figure 2. Locations of the stations (type A – surface $V_s < 1,000$ m/s, circles), type B – surface $V_s > 1,000$ m/s, triangles).

Update of SGB, CHB and SBB in CVM-S

First, we test whether a newer and higher-resolution shear wave velocity model for the SGB, CHB and the SBB constrained by ambient noise tomography (Li et al., 2023, hereafter labeled ‘SGSB’), is able to improve the fit to observed ground motions for our test events. To ensure a smooth transition where two models intersect, we used the weighting approach from Ajala and Persaud (2021) with a 15 km-wide transition zone. As shown in Figure 3, the model imaged by Li et al. (2023) as expected increases the spatial resolution within the domain covered by the ambient noise imaging, particularly in the top 1 - 2 km, while the constraints on deeper structures (3+ km) from this model are mainly for the San Gabriel basin.

Figures 4-5 show the average bias for stations located above the SGSB model for the 7 events. The effects of the SGSB model update varies for the 7 events, with the largest improvements for the La Habra, Chino Hills and El Monte events at the lower frequencies. Figure 5 (right) shows the average FAS bias for the 7 events, with a 38% improvement averaged for the 3 components for frequencies 0.2-0.5 Hz. We therefore implement the SGSB model in the CVM-S reference model in the following tests.

Calibration of Spatial Variation of GTL Depths for Type B sites

Our next step is to reassess the bias at type B sites (surface $V_s > 1,000$ m/s) that Hu et al. (2022) analyzed for the 2014 M5.1 La Habra earthquake, for the 7 earthquakes shown in Figure 1. Figures 6-12 show interpolated areal distributions of the average FAS bias at all sites for 0-1 Hz ground motion simulations of the events, using tapering depths (z_T) of 0 m (no GTL), 150 m, 300 m, 600 m, 900 m and 1,200 m (42 simulations). The FAS bias maps show that type B sites are generally underpredicted without adding the GTL for all events, which is consistent with the findings from the La Habra simulations by Hu et al. (2022). Furthermore, Figures 13-14 show average bias values for frequencies between 0.2-1.0 Hz for each event for tapering depths of 0 m (no GTL), 600 m and 1,200 m, and the average bias for all 7 events for tapering depths of 0 m, 500 m and 1,000 m. These results indicate that the optimal tapering depths for type B sites vary considerably spatially. For example, Figures 13-14 suggest that the optimal tapering depth is relatively deep (1,000-1,200 m) for the La Habra, Inglewood and San Bernardino events and about 600 m for the El Monte earthquake, while the Chino Hills event favors a very shallow GTL (near 0 m). Note, that the small number of type B sites for the Encino event (5) and to some extent the Inglewood event (12) increases the uncertainty of estimating the optimal tapering layer.

With simulations of the 7 events, we evaluated the performance of different tapering depths based on the event-averaged FAS bias values at each site, denoted as \overline{FAS}_{bias} , given by

$$\overline{FAS}_{bias}(z_T) = \frac{\sum_{i=1}^{N_{evt}} FAS_{bias,i}(z_T)}{N_{evt}},$$

where N_{evt} is the number of events. Each site thus uses up to 7 FAS bias values for each tapering depth. The estimation of the optimal tapering depth at each site is then obtained by minimizing the absolute value of the event-averaged FAS bias ($|\overline{FAS}_{bias}(z_T)|$). To further improve our estimates, we discarded sites that only recorded a single event. Compiling all the best-fit tapering

depths estimated at all the sites that qualify, we used an inverse-distance weighted interpolation to calculate a map that shows the spatially-varying tapering depth throughout our domain.

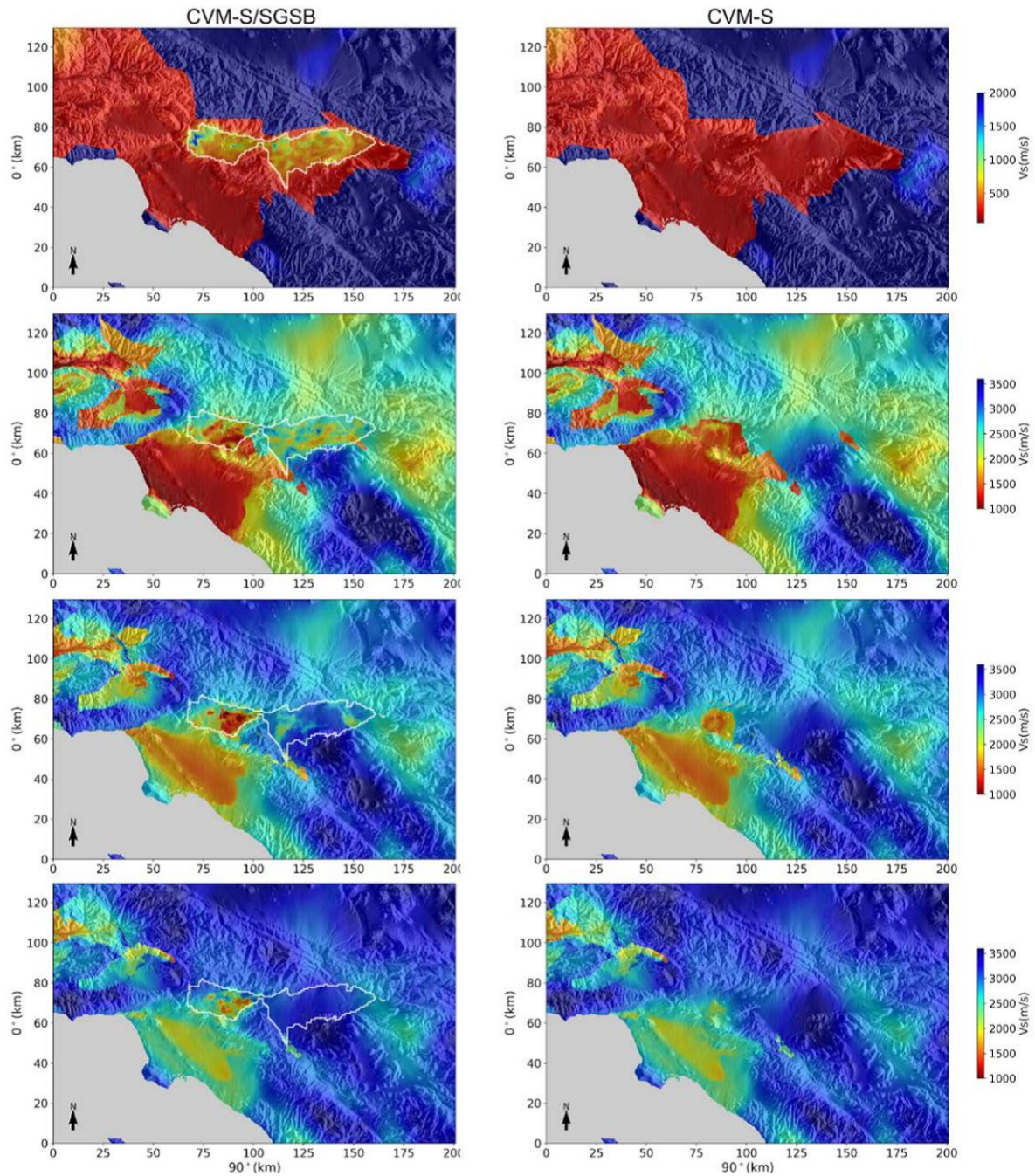


Figure 3. Horizontal slices of shear wave speeds at different depths extracted from the combined model (CVM-S/SGSB) and the original CVM-S. The white polygon in the CVM-S/SGSB model outlines the surface projection of the imaging domain of Li et al. (2023). (from top to bottom row): 0 km, 1 km, 2 km and 3 km depth.

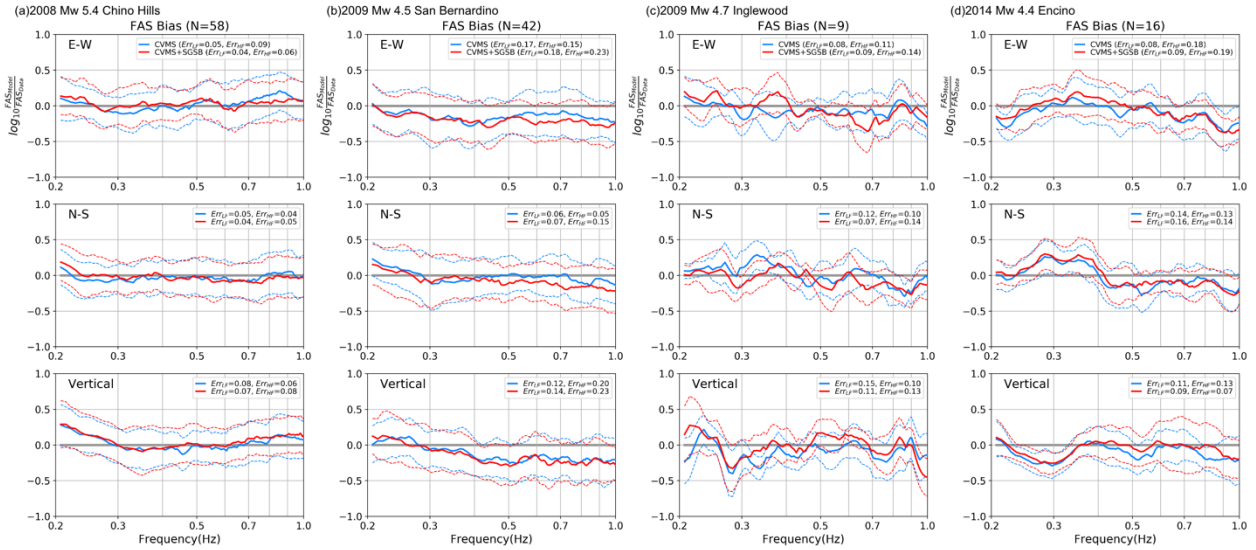


Figure 4. Comparisons of FAS bias curves derived from simulations with the original CVMSI (blue) and with CVMSI+SGSB (red), computed from all stations within the imaging domain of Li et al. (2023), for (a) the 2008 M_w 5.4 Chino Hills, (b) the 2009 M_w 4.5 San Bernardino, (c) the 2009 M_w 4.7 Inglewood, and (d) the 2014 M_w 4.4 Encino events. Err_{LF} and Err_{HF} depict the average bias for 0.2-0.5 Hz and 0.5-1.0 Hz, respectively.

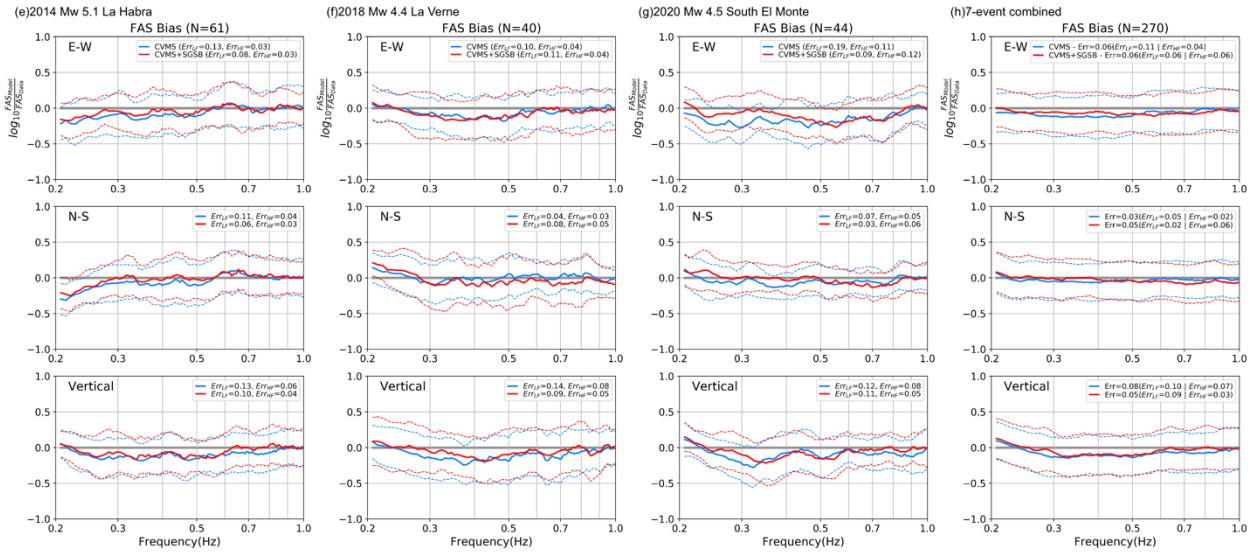


Figure 5. Same as Figure 4, but for (e) the 2014 M_w 5.1 La Habra, (f) the 2018 M_w 4.4 La Verne, (g) the 2020 M_w 4.5 South El Monte events, and (h) the average bias for all 7 events.

Figure 15 shows the estimated GTL tapering depth, inferred from the maps of average 0.3-1.0 Hz FAS combined for the 7 events shown in Figure 1, at the 348 sites with two or more measurements. For type B sites (triangles), as indicated by the individual events (Figures 6-12), the optimal tapering depth shows strong spatial variation. In general, the optimal tapering depths appear to be near 0 m just outside the basins, and increase away from the basins up to distances of about 10-50 km modeled here, in particular toward the northeast, east and southeast.

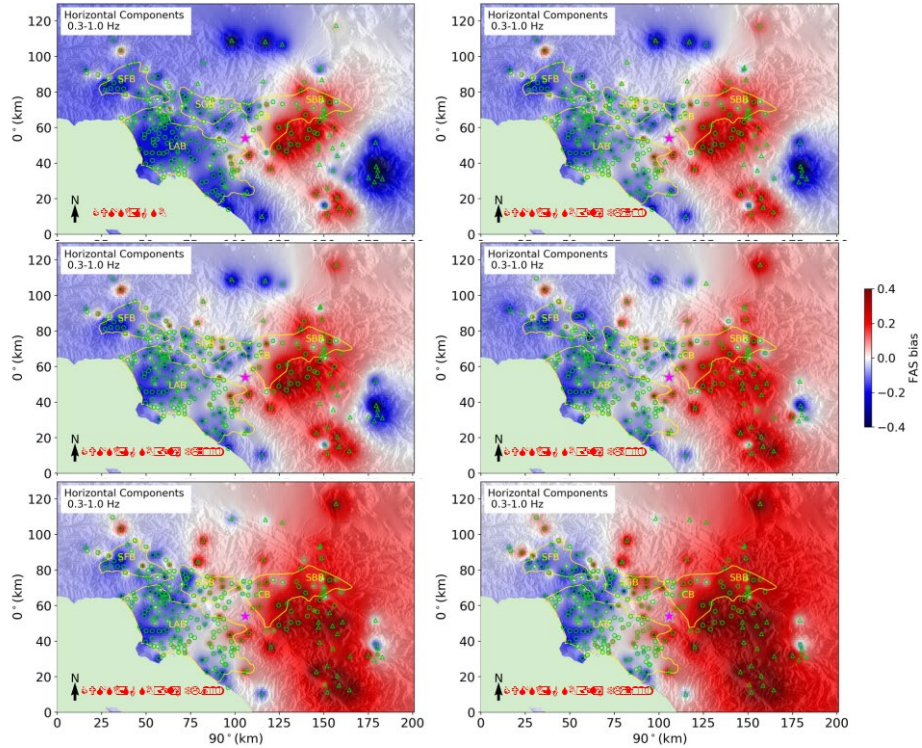


Figure 6. 0.3-1.0 Hz FAS bias at sites for the 2008 M_w 5.4 Chino Hills earthquake with GTL depths of 0 m, 150 m, 300 m, 600 m, 900 m and 1200 m. The yellow lines depict approximate outlines of the SFB, LAB, SGB, CB, and SBB.

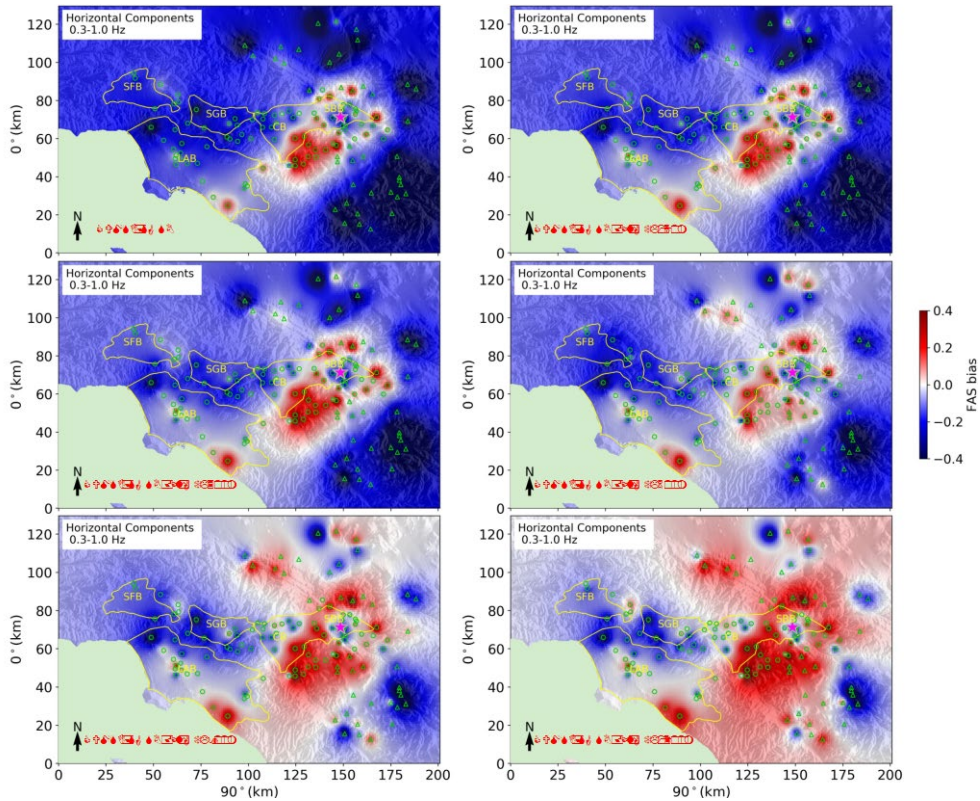


Figure 7. Same as Fig. 6, but for the 2009 M_w 4.5 San Bernardino earthquake.

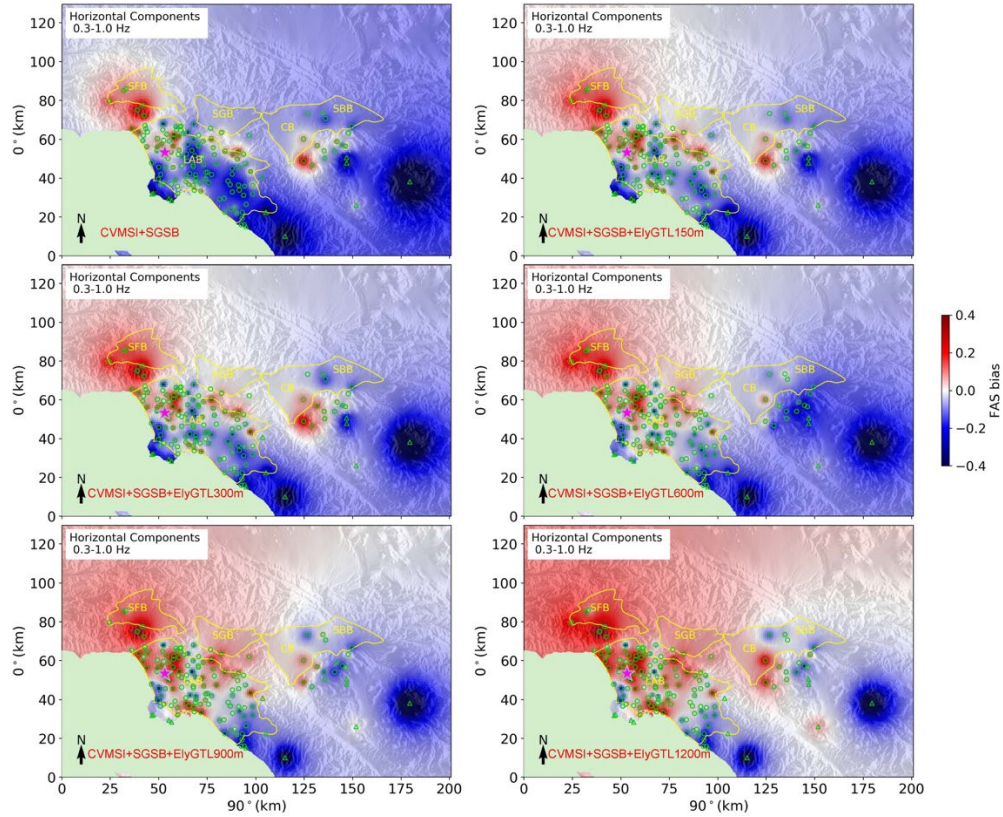


Figure 8. Same as Fig. 6, but for the 2009 M_w 4.7 Inglewood earthquake.

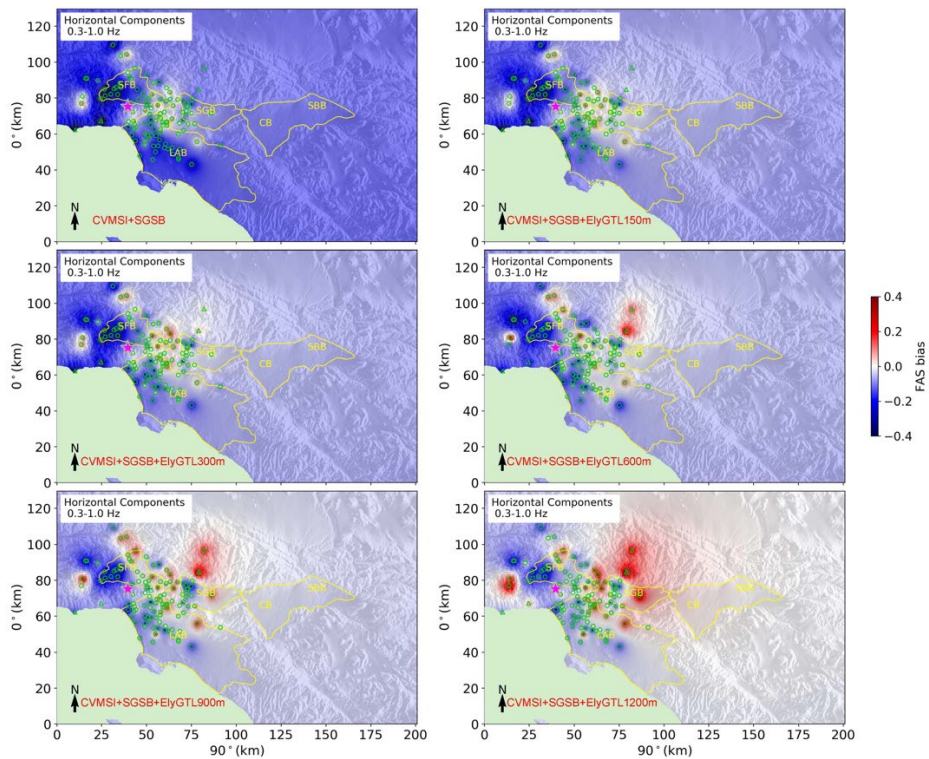


Figure 9. Same as Fig. 6, but for the 2014 M_w 4.4 Encino earthquake.

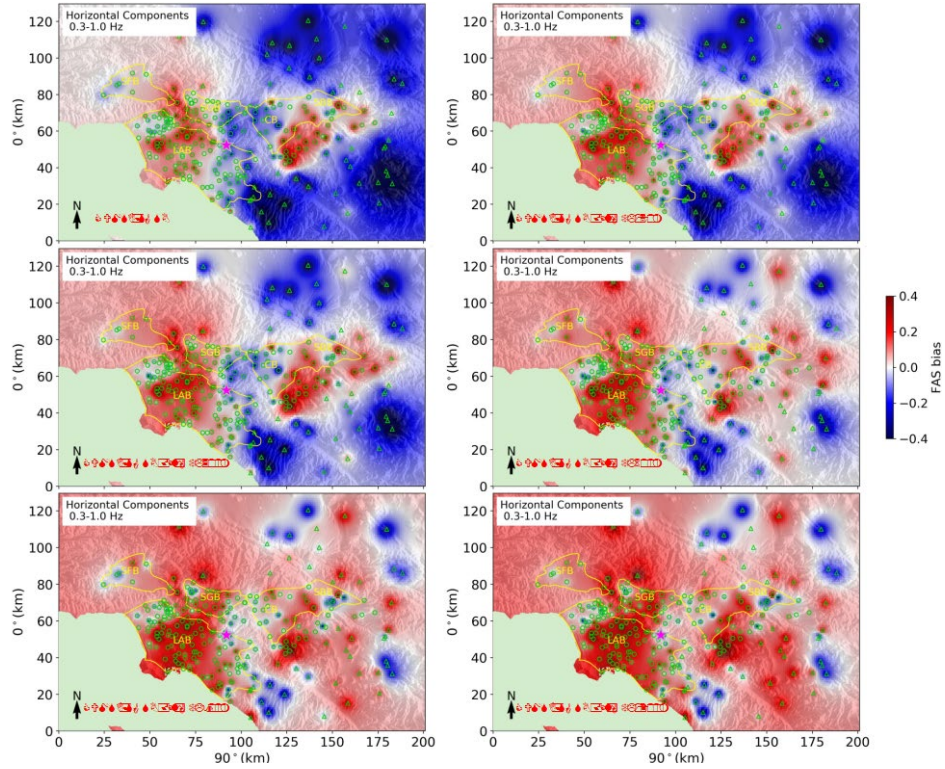


Figure 10. Same as Fig. 6, but for the 2014 M_w 5.1 La Habra earthquake.

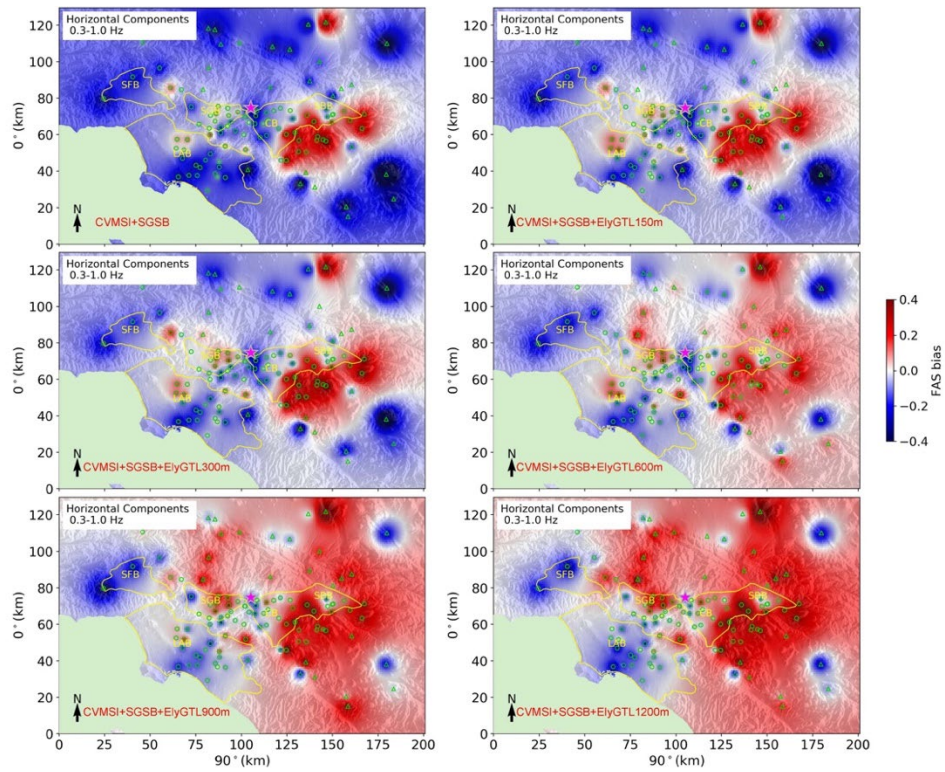


Figure 11. Same as Fig. 6, but for the 2018 M_w 4.4 La Verne earthquake.

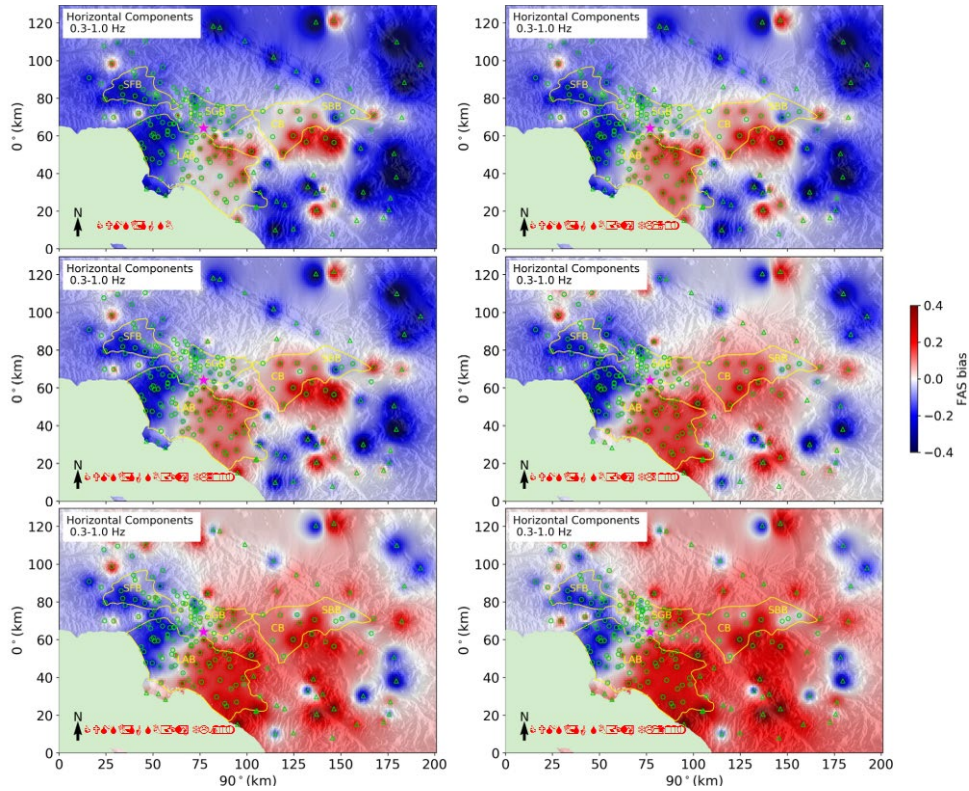


Figure 12. Same as Fig. 6, but for the 2020 M_w 4.5 South El Monte earthquake.

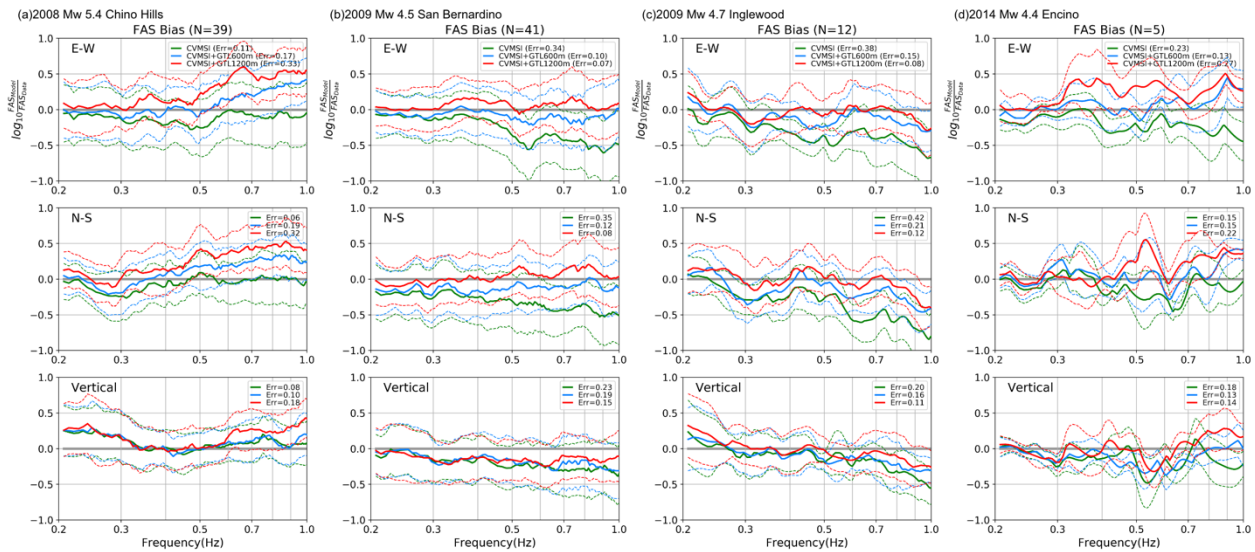


Figure 13. 0.2-1.0 Hz FAS bias at type B sites for (a) the 2008 M_w 5.4 Chino Hills earthquake, (b) the 2009 M_w 4.5 San Bernardino earthquake, (c) the 2009 M_w 4.7 Inglewood earthquake, and (d) the 2014 M_w 4.4 Encino earthquake, with no GTL (green lines), a 600 m GTL (blue lines), and a 1200 m GTL (red lines). ‘N’ depicts the number of type B sites.

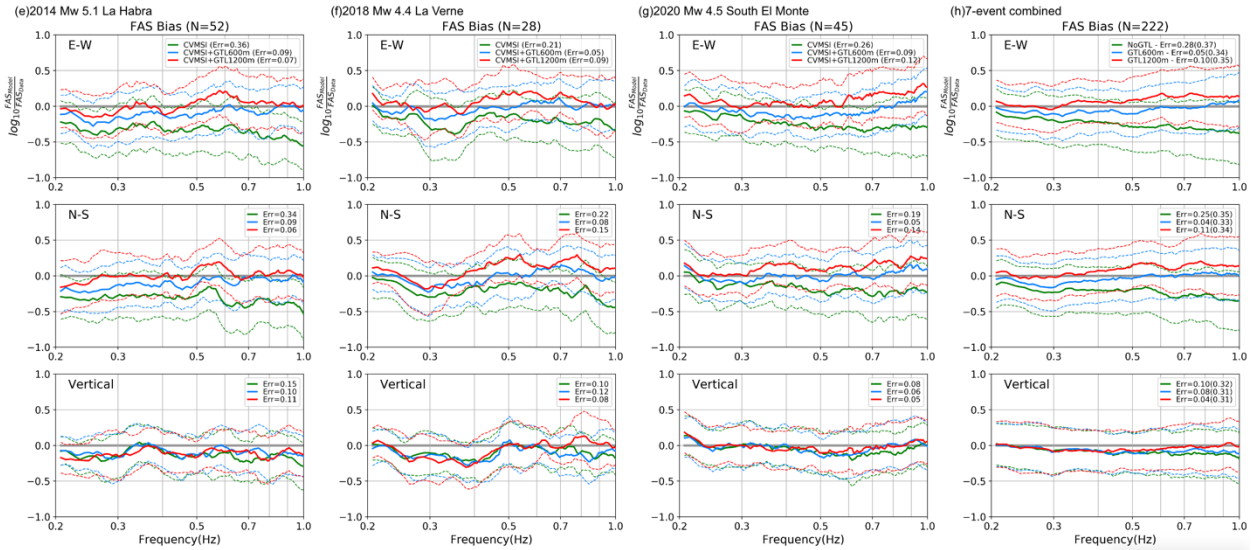


Figure 14. Same as Figure 13, but for (e) the 2014 M_w 5.1 La Habra earthquake, (f) the 2018 M_w 4.4 La Verne earthquake, (g) the M_w 4.5 South El Monte earthquake, and (h) average for all 7 events.

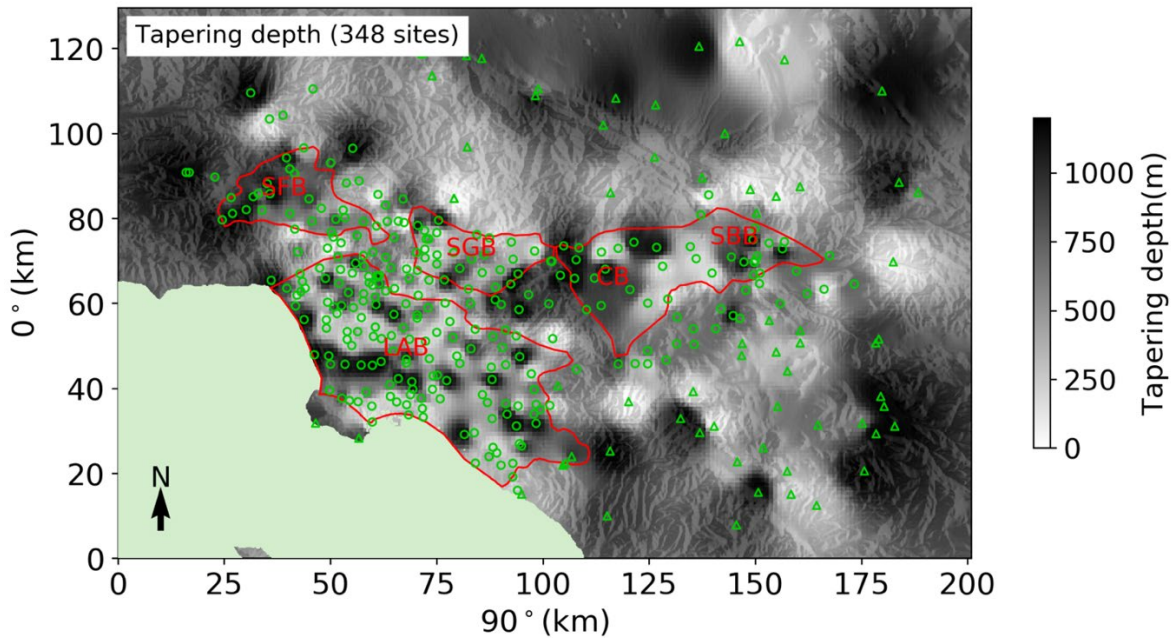


Figure 15. Estimated tapering depth of the GTL, inferred from the maps of average 0.3-1.0 Hz FAS bias for the 7 events shown in Figure 1. The red lines depict approximate outlines of the San Fernando basin (SFB), Los Angeles basin (LAB), San Gabriel basin (SGB), Chino basin (CB), and San Bernardino basin (SBB).

Figure 16 shows the FAS bias of a simulation of the 2014 M_w 5.1 La Habra earthquake, including the spatially-variable distribution of optimal GTL depths found in Fig. 15, but for type

B sites only. The FAS bias is generally removed outside the basins, except for isolated sites with strong under- or overprediction, which requires further analysis in future work.

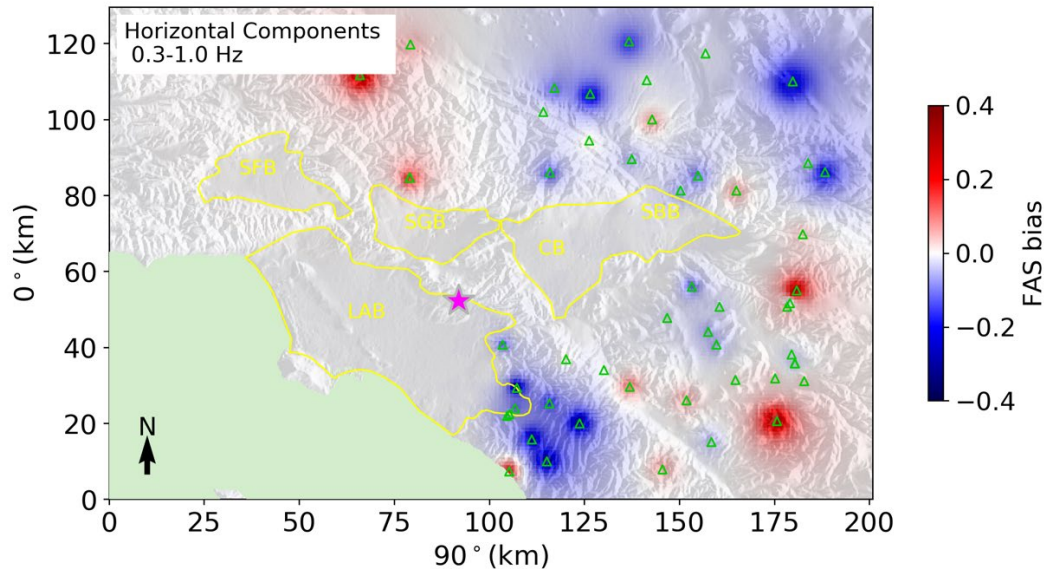


Figure 16. Average FAS bias for the 2014 M5.1 La Habra event in a model including spatially-variable GTL depths for type B sites only.

Discussion and conclusions

We have shown that incorporating a new model of the San Gabriel, Chino and San Bernardino basins obtained from ambient noise tomography into the SCEC CVM-S decreases the FAS bias between 3D physics-based simulations and strong motion data by 38% for 7 M_w 4.4-5.4 earthquakes at sites directly above the model for frequencies 0.2-0.5 Hz. We then use the updated CVM to estimate the depth distribution of a near-surface GTL that minimizes the average 0.3-1.0 Hz FAS bias between the simulations and strong motion data in the greater Los Angeles area, CA. For sites with shear-wave velocity larger than 1,000 m in the CVM, the optimal tapering depth shows strong spatial variation. In general, the optimal tapering depths appear to increase from near 0 m at the edges of the sedimentary basins to values of 1,000 m or larger at distances of 10-50 km from the basins, in particular toward the northeast, east and southeast. A simulation of the 2014 La Habra event with this distribution of spatially-variable optimal GTL depths shows an improved fit between synthetics and data for type B sites, leaving only isolated sites with strong under- or overprediction.

Hu et al. (2022) applied their GTL modifications only where existing V_s values were larger than the proposed taper, arguing that the SCEC CVM-S is already well-constrained by well data, V_{s30} values, etc, inside the basins. However, while this study focused on estimating the optimal GTL thickness at sites outside the sedimentary basins, our simulations also applied the GTL taper at sites inside the basins (see Figure 15). The basin sites generally favor small to no (additional) GTL in the SCEC CVM-S, while some sites show a rapid spatial variation between 0 m and 1,200 m, many aligned along pseudo-linear trends. We recommend further scrutiny on the V_s profiles at the basin sites in the SCEC CVM-S in order to improve the fit between seismic synthetics and data.

Acknowledgements

This research was supported by the California Geological Survey (Award #1022-003).

References

- Ajala, R., and P. Persaud (2021). Effect of merging multiscale models on seismic wavefield predictions near the southern San Andreas Fault. *J. Geophys. Res.* **126**, no. 10, e2021JB021915, doi: [10.1029/2021JB021915](https://doi.org/10.1029/2021JB021915).
- Cui, Y., Poyraz, E., Olsen, K. B., Zhou, J., Withers, K., Callaghan, S., Larkin, J., Guest, C., Choi, D., Chourasia, A., et al. (2013). Physics-based seismic hazard analysis on petascale heterogeneous supercomputers. Page 70 of: Proceedings of SC13: International Conference for High Performance Computing, Networking, Storage and Analysis. ACM.
- Boore, D. M., and W. B. Joyner (1997). Site amplifications for generic rock sites. *Bull. Seismol. Soc. Am.* **87**, no. 2, 327–341, doi: [10.1785/BSSA0870020327](https://doi.org/10.1785/BSSA0870020327).
- Brocher, T. M. (2005) Empirical Relations between Elastic Wave speeds and Density in the Earth's Crust. *Bull. Seismol. Soc. Am.* **95**, no. 6, 2081–2092, doi: [10.1785/0120050077](https://doi.org/10.1785/0120050077).
- Ely, G. P., Jordan, T., Small, P., and Maechling, P. J. (2010). A Vs30-derived near-surface seismic velocity model. AGU Fall Meet., San Francisco, California, 13–17 December, Abstract.
- Hu, Z., K.B. Olsen, and S.M. Day (2022). Calibration of the Near-surface Seismic Structure in the SCEC Community Velocity Model Version 4. *Geophys. Jour. Int.* **230**, 2183-2198.
- Konno, K., and T. Ohmachi (1998). Ground-motion characteristics estimated from spectral ratio between horizontal and vertical components of microtremor. *Bull. Seismol. Soc. Am.* **88**, no. 1, 228–241, doi: [10.1785/BSSA0880010228](https://doi.org/10.1785/BSSA0880010228).
- Li, Y., V. Villa, R.W. Clayton, and P. Persaud (2023). Shear wave velocities in the San Gabriel and San Bernardino Basins, California. *Jour. Geophys. Res., Solid Earth* **128**(7).
- Nie, S., Wang, Y., Olsen, K. B., and Day, S. M. (2017). Fourth Order Staggered Grid Finite Difference Seismic Wavefield Estimation Using a Discontinuous Mesh Interface (WEDMI). *Bull. Seism. Soc. Am.* **107**(5), 2183-2193.
- Olsen, K.B. (2000). Site Amplification in the Los Angeles Basin from 3D Modeling of Ground Motion. *Bull. Seis. Soc. Am.* **90**, S77-S94.
- Olsen, K.B., Day, S.M., and C.R. Bradley (2003). Estimation of Q for long-period (>2 s) waves in the Los Angeles Basin. *Bull. Seis. Soc. Am.* **93**, 627-638.
- O'Reilly, O., T.-Y. Yeh, K.B. Olsen, Z. Hu, A. Breuer, D. Roten, and C. Goulet (2022). A high-order finite difference method on staggered curvilinear grids for seismic wave propagation applications with topography. *Bull. Seis. Soc. Am.* **112** (1), 3-22, <https://doi.org/10.1785/0120210096>.
- Shao, G., C. Ji and E. Hauksson (2012). Rupture process and energy budget of the 29 July 2008 Mw 5.4 Chino Hills, California, earthquake, *J. geophys.,Res. Solid Earth*, **117**(B7), doi:[10.1029/2011JB008856](https://doi.org/10.1029/2011JB008856).
- Small, P., D. Gill, P. Maechling, R. Taborda, S. Callaghan, T.H. Jordan, et al. (2017). The SCEC Unified Community Velocity Model Software Framework. *Seismol. Res. Lett.*, **88**(6), 1539-1552. <https://doi.org/10.1785/0220170082>
- Thompson, E. M. (2018). An Updated Vs30 Map for California with Geologic and Topographic Constraints, US Geol. Surv. Data Release, doi: [10.5066/F7JQ108S](https://doi.org/10.5066/F7JQ108S).